

ADVERTISEMENT

PLOS Computational Biology  
Macromolecular Structure and Dynamics Collection

**PLOS**  
OPEN ACCESS

[plos.org](http://plos.org)[create account](#)[sign in](#)[Browse](#)[Publish](#)[About](#)[Search](#)[advanced search](#)

January 28, 2016

# Spontaneous Decoding of the Timing and Content of Human Object Perception from Cortical Surface Recordings Reveals Complementary Information in the Event-Related Potential and Broadband Spectral Change

*Image credit: Miller et al.*

**TEN SIMPLE RULES ARTICLE** 01/28/2016

**Ten Simple Rules for a Bioinformatics Journal Club**

**WHAT'S WITH ALL THE PIE CHARTS?**

In the field of bioinformatics, expertise may be spread across departments and institutions, and there may not be an obvious place or critical mass in any one lab for a traditional journal club. Lonsdale et al. offer an alternative—an informal journal club, designed to bring together a diversity of backgrounds and career stages to discuss bioinformatics while building a network of like-minded peers.

*Image credit: Lonsdale et al.*

**RECENTLY PUBLISHED ARTICLES**

Binding Site Identification and Flexible Docking of Single Stranded RNA to...

A Computational Model for the AMPA Receptor Phosphorylation Master Switch...

Does High-Dose Antimicrobial Chemotherapy Prevent the Evolution of...

[SEE ALL ARTICLES](#)

**CURRENT ISSUE**  
December 2015

**RESEARCH ARTICLE** 01/28/2016

**Does High-Dose Antimicrobial Chemotherapy Prevent the Evolution of Resistance?**

High-dose chemotherapy has long been advocated as a means of controlling drug resistance in infectious diseases, but recent empirical studies have begun to challenge this view. Troy Day and Andrew F. Read develop a general framework for modeling and understanding resistance emergence based on principles from evolutionary biology.

*Image credit: Jamie Dobson/Flickr*

**REVIEW ARTICLE** 01/21/2016

**Computational Modeling, Formal Analysis, and Tools for Systems Biology**

Bartocci and Lió discuss the most important and exciting computational methods and tools currently available to systems biologists. The authors believe that a deeper understanding of the concepts and theory highlighted in this review will produce better software practice, improved investigation of complex biological processes, and even new ideas and better feedback into computer science.

*Image credit: PLOS*

**RESEARCH ARTICLE** 01/25/2016

**Social Norms of Cooperation in Small-Scale Societies**

Cooperation, reciprocity and the art of managing reputations, have been features of human interaction from their pre-historic existence in small-scale societies to contemporary times, when technology supports interaction with large numbers of people. Santos et al. present a mathematical framework to analyze the relationship between different social norms and the sustainability of cooperation.

*Image credit: Patrick Gruber/ Flickr*

**Publish with PLOS**[Submission Instructions](#)[Submit Your Manuscript](#)**Connect with Us**[PLOS Blogs](#)**RESEARCH ARTICLE****Binding Site Identification and Flexible Docking of**

## RESEARCH ARTICLE

# Spontaneous Decoding of the Timing and Content of Human Object Perception from Cortical Surface Recordings Reveals Complementary Information in the Event-Related Potential and Broadband Spectral Change

CrossMark  
click for updates

## OPEN ACCESS

**Citation:** Miller KJ, Schalk G, Hermes D, Ojemann JG, Rao RPN (2016) Spontaneous Decoding of the Timing and Content of Human Object Perception from Cortical Surface Recordings Reveals Complementary Information in the Event-Related Potential and Broadband Spectral Change. PLoS Comput Biol 12(1): e1004660. doi:10.1371/journal.pcbi.1004660

**Editor:** Olaf Sporns, Indiana University, UNITED STATES

**Received:** May 26, 2015

**Accepted:** November 17, 2015

**Published:** January 28, 2016

**Copyright:** © 2016 Miller et al. This is an open access article distributed under the terms of the [Creative Commons Attribution License](#), which permits unrestricted use, distribution, and reproduction in any medium, provided the original author and source are credited.

**Data Availability Statement:** The authors confirm that all data underlying the findings are fully available without restriction. All data and analyses are available at <https://purl.stanford.edu/xd109qh3109>

**Funding:** This work was supported by National Aeronautics and Space Administration Graduate Student Research Program (KJM), the NIH (R01-NS065186 (KJM, JGO, RPNR), T32-EY20485 (DH), R01-EB00856 (GS) and P41-EB018783 (GS)), the NSF (EEC-1028725 (RPNR)), and the US Army

Kai J. Miller<sup>1,2,3\*</sup>, Gerwin Schalk<sup>4</sup>, Dora Hermes<sup>5</sup>, Jeffrey G. Ojemann<sup>3,6,7</sup>, Rajesh P. N. Rao<sup>3,7,8</sup>

**1** Departments of Neurosurgery, Stanford University, Stanford, California, United States of America, **2** NASA —Johnson Space Center, Houston, Texas, United States of America, **3** Program in Neurobiology and Behavior, University of Washington, Seattle, Washington, United States of America, **4** National Center for Adaptive Neurotechnologies, Wadsworth Center, New York State Department of Health, Albany, New York, United States of America, **5** Psychology, Stanford University, Stanford, California, United States of America, **6** Department of Neurological Surgery, University of Washington, Seattle, Washington, United States of America, **7** Center for Sensorimotor Neural Engineering, University of Washington, Seattle, Washington, United States of America, **8** Computer Science and Engineering, University of Washington, Seattle, Washington, United States of America

\* [kai.miller@stanford.edu](mailto:kai.miller@stanford.edu)

## Abstract

The link between object perception and neural activity in visual cortical areas is a problem of fundamental importance in neuroscience. Here we show that electrical potentials from the ventral temporal cortical surface in humans contain sufficient information for spontaneous and near-instantaneous identification of a subject's perceptual state. Electrocorticographic (ECoG) arrays were placed on the subtemporal cortical surface of seven epilepsy patients. Grayscale images of faces and houses were displayed rapidly in random sequence. We developed a template projection approach to decode the continuous ECoG data stream spontaneously, predicting the occurrence, timing and type of visual stimulus. In this setting, we evaluated the independent and joint use of two well-studied features of brain signals, broadband changes in the frequency power spectrum of the potential and deflections in the raw potential trace (event-related potential; ERP). Our ability to predict both the timing of stimulus onset and the type of image was best when we used a combination of both the broadband response and ERP, suggesting that they capture different and complementary aspects of the subject's perceptual state. Specifically, we were able to predict the timing and type of 96% of all stimuli, with less than 5% false positive rate and a ~20ms error in timing.

Research Office (W911NF-14-1-0440 (GS)). The funders had no role in study design, data collection and analysis, decision to publish, or preparation of the manuscript.

**Competing Interests:** The authors have declared that no competing interests exist.

## Author Summary

We describe a new technique for decoding perception from electrical potentials measured from the human brain surface. All previous attempts have focused on the identification of classes of stimuli or behavior where the timing of experimental parameters is known or pre-designated. However, real world experience is spontaneous, and to this end we describe an experiment predicting the occurrence, timing, and types of visual stimuli perceived by human subjects from the continuous brain signal. In this experiment, human patients with electrodes implanted on the underside of the temporal lobe were shown pictures of faces and houses in rapid sequence. We developed a novel template-projection method for analyzing the electrical potentials, where, for the first time, broadband spectral changes and raw potential changes could be contrasted as well as combined. Our analyses revealed that they carry different physiological information, and, when used together, allow for unprecedented accuracy and precision in decoding human perception.

## Introduction

How does a two-dimensional pattern of pixels measured by our retina get transformed into the percept of a friend's face or a famous landmark? It is known that the ventral temporal cortex represents different classes of complex visual stimuli within distinct regions. For example, category-selective areas have been established unambiguously at scale of several millimeters using functional imaging and macroscale field potentials [1–4]. Similar results have also been demonstrated at the single-unit level in epileptic human patients [5] and non-human primates [6]. More recently, high frequency electrocorticographic (ECoG) changes from these same ventral temporal regions have been shown to increase while viewing images of faces, places, and other objects [7–10]. However, rather than reflecting a discrete range of frequencies, >40Hz ECoG changes have been shown to instead be a reflection of broadband fluctuations across the entire frequency domain [11,12], and these broadband changes show robust increases across ventral temporal cortex during object perception [13].

Object-category specific responses in inferotemporal cortex were initially identified using event-related potentials (ERPs) in ECoG [14,15] or functional magnetic resonance imaging (fMRI) [1–4] although little spatial overlap was found between the ERP and the fMRI response [16]. In contrast, increases in high-frequency broadband power in cortical surface potentials recorded using ECoG matched well with the category-specific fMRI responses in the inferior temporal cortex [17,18]. The ERP and broadband signals show distinct, and partially overlapping, responses to faces [13,19] (Fig 1), but it is unclear whether the information content is itself distinct between the two. While both the ERP and the raw ECoG potential have previously been used to classify object categories [20–22], these studies required knowledge about the time of stimulus onset, rather than determining them spontaneously. Furthermore, the ability of the algorithms to establish object category from neural data was well below that of human performance (both in terms of accuracy and temporal fidelity).

A significant methodological obstacle to this type of macroscale physiology has been the difficulty interpreting heterogeneity in response morphologies. As illustrated in Fig 1, face-selective ERPs may have wide structural variation, with "peaks" and "troughs" that are very different in shape, latency, and duration, even when measured from brain sites separated by only 1cm. It remains unclear what the ERP shape actually corresponds to. Furthermore, methodology has not previously been developed to naively place morphologically-diverse ERPs in a common feature space. In contrast, broadband spectral changes in the ECoG signal have been

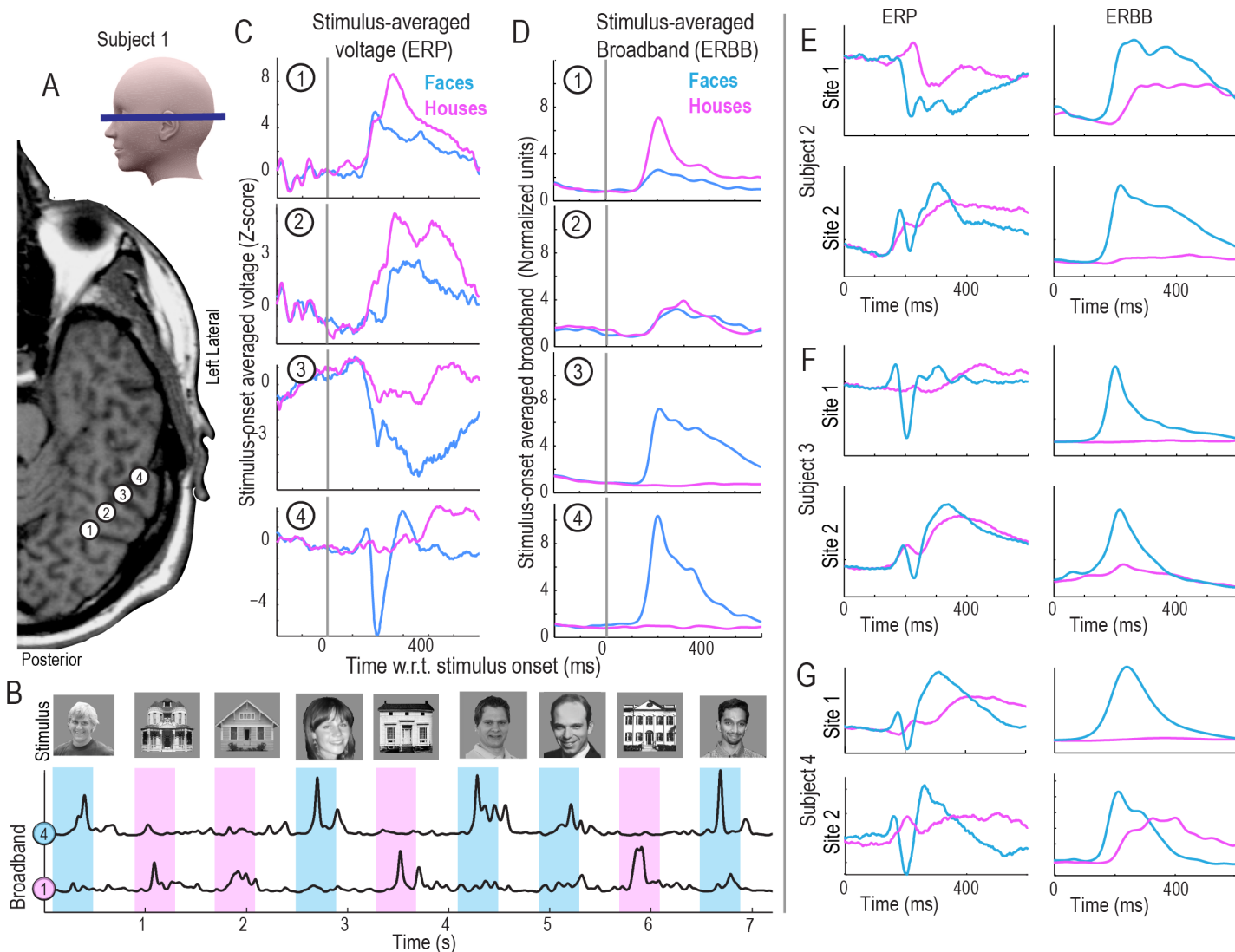


**Fig 1. The basic face and house discrimination task, and the polymorphic nature of the electrophysiologic response.** (A) Subdural electrocorticographic (ECOG) electrode strips were placed through burrholes in the skull onto ventral temporal brain surface. 4 adjacent sites are shown for subject 1. (B) Simple luminance- and contrast-matched grayscale faces and houses that were displayed in random order for 400ms each, with 400ms blank gray screen inter-stimulus interval between each picture. Subjects were asked to report a simple target (an upside-down house, which was rejected from analyses). From the raw potential, the time course of broadband spectral change was extracted from each brain site (here sites 1&4 from (A)). Blue = faces; pink = houses. (C) The averaged raw potential (ERP) following face (blue) and house (pink) stimuli for the 4 sites in (A). (D) The averaged broadband power following different stimuli (ERBB—a reflection of averaged neuronal firing rate), from sites 1–4 in (A). (E–G) ERBB and ERP for 2 sites over fusiform gyrus in subjects 2–4. Note that the responses are highly polymorphic for the event-related potentials, and that there are ERP face-selective sites that do not have the classic N200 shape. As seen for site 2 in Subject 4, the classic N200, when present, does not guarantee face-selectivity in the ERBB.

doi:10.1371/journal.pcbi.1004660.g001

shown to correlate with neuronal firing rate [23,24], although it has been unclear how ERPs relate to this, or what the best way to attempt such a comparison is [19]. Our work begins by describing a template-projection technique, where templates of averaged raw potentials (ERPs) and broadband changes (ERBB) from a training period are projected into the data from a testing period. This places ERP and ERBB features from different brain sites into a common feature space, where they can be directly compared with one another, and used together for decoding brain function.

To date, decoding of perceptual content has relied upon designated information about external stimuli, where the frequency of occurrence and precise timing are known to the decoder. We propose that in addition to identifying the perceptual content (e.g. image type), decoding of the brain state should evolve to spontaneously identify whether a perceptual event has happened from the datastream, and, if so, predict the timing as accurately as possible. We denote this practice as “spontaneous decoding”.

Here we show that the ECoG signal contains sufficient information to allow near-instantaneous identification of object categories with an accuracy comparable to that of human behavioral performance. Our experiments measured ECoG recordings from several inferior temporal visual areas simultaneously while subjects viewed randomly interleaved images of faces or houses. We achieved the best results by combining broadband changes with raw potential changes (rather than with either independently), using a template projection approach. This shows that the two types of signals capture complementary aspects of the physiology reflecting a human subject’s perceptual state. With this combination, we were able to predict 96% of all stimuli correctly as face, house, or neither, with only ~20 ms error in timing.

## Methods

### Ethics statement

All patients participated in a purely voluntary manner, after providing informed written consent, under experimental protocols approved by the Institutional Review Board of the University of Washington (#12193). All patient data was anonymized according to IRB protocol, in accordance with HIPAA mandate. A portion of this data appears in a different context in [13]. All data and analyses are publically available at <http://purl.stanford.edu/xd109qh3109>.

### Subjects and recordings

All 7 subjects in the study were epileptic patients ([S1 Table](#)) at Harborview Hospital in Seattle, WA. Subdural grids and strips of platinum electrodes (Ad-Tech, Racine, WI) were clinically placed over frontal, parietal, temporal, and occipital cortex for extended clinical monitoring and localization of seizure foci. Lateral frontoparietal electrode grids were discarded from analysis, and only strip electrodes were further considered. The electrodes had 4 mm diameter (2.3 mm exposed), 1 cm inter-electrode distance, and were embedded in silastic. Electrode locations relative to gyral surface anatomy were determined by projection of the post-implant CT to the pre-operative axial T1 using normalized mutual information in SPM, and the CTMR package, with Freesurfer-extracted cortical surface mesh reconstructions [25–28]. When the MRI or CT was of insufficient quality, hybrid techniques were used [29].

Experiments were performed at the bedside, using Synamps2 amplifiers (Neuroscan, El Paso, TX) in parallel with clinical recording. Stimuli were presented with a monitor at the bedside using the general-purpose BCI2000 stimulus and acquisition program [30]. The electrocorticographic potentials were measured with respect to a scalp reference and ground, subjected to an instrument-imposed bandpass filter from 0.15 to 200 Hz, and sampled at 1000 Hz.

To reduce common artifacts, the potential,  $V_n^0(t)$ , measured at time  $t$  in each electrode  $n$ , was re-referenced with respect to the common average of all  $N$  electrodes,

$$V_n(t) = V_n^0(t) - \frac{1}{N} \sum_{i=1}^N V_i^0(t).$$

Electrodes with significant artifact or epileptiform activity were

rejected prior to common averaging. There was no rejection of epochs of time within the data. Ambient line noise was rejected by notch filtering between 58–62 Hz using a 3<sup>rd</sup>-order Butterworth filter [31].

### Face-House discrimination task

Subjects performed a basic face and house stimulus discrimination task. They were presented with grayscale pictures of faces and houses (luminance- and contrast-matched) that were displayed in random order for 400ms each, with 400ms blank screen inter-stimulus interval (ISI) between the pictures. The 10cm-wide pictures were displayed at ~1m from the patients while they were seated at the bedside (Fig 1). There were 3 experimental runs with each patient, with 50 house pictures and 50 face pictures in each run (for a total of 300 stimuli). In order to maintain fixation on the stimuli, patients were asked to verbally report a simple target (an upside-down house), which appeared once during each run (1/100 stimuli). There were few errors in reporting the upside-down target house in any run (approximately 2–3 across all 21 experimental runs).

### Power spectral analysis, and decoupling the dynamic power spectrum to obtain the timecourse of broadband spectral change (fully detailed in the Supplemental material, [S1 Text](#) and [S2 Text](#))

Following previously described methodology [11,32,33], we perform discrete estimates of the windowed power spectrum, as well as a time-frequency approximation of the dynamic power spectrum from  $V_n(t)$ . We then perform a “decoupling process” to identify underlying motifs in power-spectral change, isolating the timecourse of broadband spectral change,  $B_n(t)$ . This process was originally described and illustrated in full detail for ECoG recordings from motor cortex [11], and later illustrated specifically for this face-house context [12]. Broadband changes have been shown to robustly characterize the magnitude and latency of cortical dynamics from ventral temporal cortex, in single trials, during this face and house viewing experiment [13]. Generically, the broadband power time course is meant to function as a time-varying estimate of changes in a multiplicative factor of the population firing rate [11,24].

### Decoding

**Cross-validation.** Prior to further analysis, the data were divided into thirds temporally (e.g. divided into experimental runs). Subsequent analyses were then performed in a 3-fold fashion. In each cross-fold, two thirds (two runs) of the data were assigned to a “**training**” set, and the remaining third was assigned to a “**testing**” set (In bold throughout for emphasis). In this way, all data could be used for both testing as well as training, but never at the same time (to maximize use without “double-dipping”, which is simultaneously testing and training on the same data). However, the spectral decoupling process was performed only once, across all data, rather than cross-folded (the decoupling process is ignorant of class-labels, or timepoint selection).

**Template projection technique.** *Stimulus triggered averaged raw potential and broadband template:* In each electrode  $n$ , stimulus-triggered averages of the training data were obtained for the common-averaged electric potential for the face ( $S \rightarrow F$ ) and house ( $S \rightarrow H$ ) stimuli independently ( $\tau_{k_s}$  denotes the  $k^{th}$  of  $N_S$  total instances of stimulus type  $S$  in the training set):

$$\langle V_n(t') \rangle_S^0 = \frac{1}{N_S} \sum_{k_s=1}^{N_S} V_n(\tau_{k_s} + t').$$

This quantity is only calculated on the peri-stimulus interval  $-199 < t' \leq 400$  ms (where  $t'$  denotes time with respect to stimulus start). It is then re-centered by subtracting the average potential peri-stimulus baseline on the interval  $-199 < t' \leq 50$ , (50ms post-stimulus is chosen to correspond with ERP and broadband ECoG latency to primary visual cortex [33,34]) to

obtain  $\langle V_n(t') \rangle_S$ :

$$\langle V_n(t') \rangle_S = \langle V_n(t') \rangle_S^0 - \frac{1}{250} \sum_{t''=-199}^{50} \langle V_n(t'') \rangle_S^0$$

We perform the same averaging over the **training data** for the broadband signal to obtain  $\langle B_n(t') \rangle_S$ . Examples of these response templates,  $\langle V_n(t') \rangle_S$  and  $\langle B_n(t') \rangle_S$  are illustrated throughout the manuscript.

#### Projection of templates into pre-defined times of stimuli onset (illustrated in Fig 2).

$\langle V_n(t') \rangle_S$  and  $\langle B_n(t') \rangle_S$  were generated from the **training period**.

**Training feature points** were obtained by **back-projecting**  $\langle V_n(t') \rangle_S$  and  $\langle B_n(t') \rangle_S$  into the **training period** to obtain sets  $\Gamma_{n,S}^V(q)$  and  $\Gamma_{n,S}^B(q)$  for each event  $q$  at time  $\tau_q$ :

$$\Gamma_{n,S}^V(q) = \sum_{t'=199}^{400} \langle V_n(t') \rangle_S (V_n(\tau_q + t') - \overline{V_n^b(\tau_q)}), \text{ where } \overline{V_n^b(\tau_q)} \text{ represents an "instantaneous" baseline surrounding time } \tau_q: \overline{V_n^b(\tau_q)} = \sum_{t=-199}^{50} V_n(t + \tau_q).$$

$\Gamma_{n,S}^B(q)$  were obtained in the same fashion. The training event types  $q$  were face picture stimulus onset ( $q \rightarrow F$ ), house picture stimulus onset ( $q \rightarrow H$ ), or randomly chosen points during the inter-stimulus interval (ISI,  $q \rightarrow o$ ), with 4 during each ISI period, at least 100ms from stimulus offset/onset and 50ms from one another.

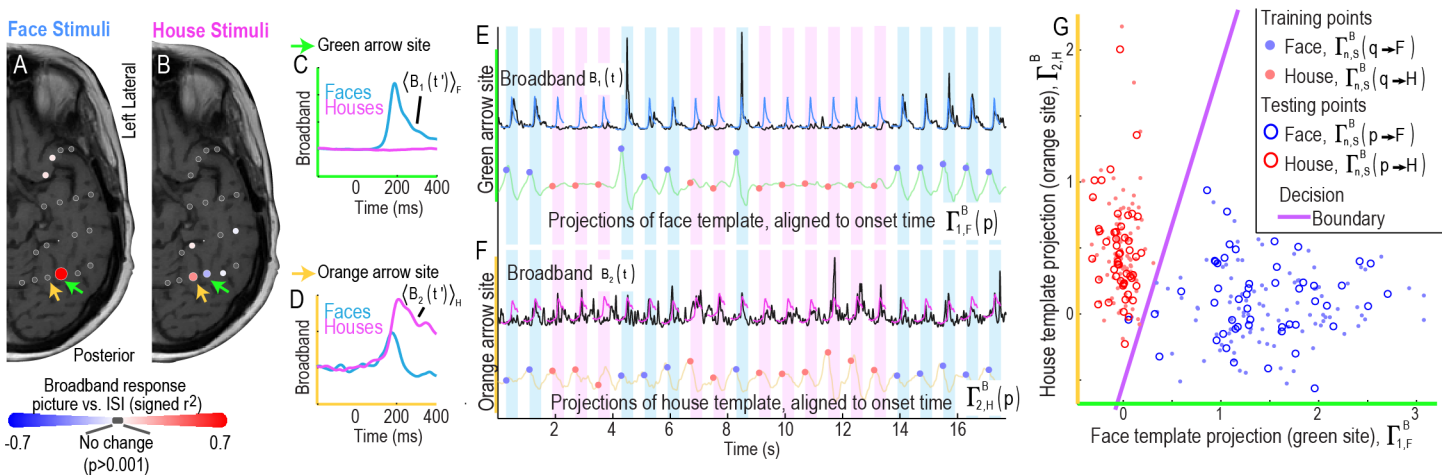


**Fig 2. Decoding the stimulus class in single trials when the onset of a stimulus is known, subject 3.** (A) Squared cross-correlation values at each electrode. **Training feature points** were obtained by back-projecting the event triggered broadband,  $\langle B_n(t') \rangle_F$  (see Methods), into the training data and comparing projected face,  $\Gamma_{n,F}^B(q \rightarrow F)$ , and inter-stimulus interval (ISI),  $\Gamma_{n,F}^B(q \rightarrow o)$ , points. These  $r_n^2$  values are scaled by color, and plotted on an axial MRI slice with scaling shown in the colored bar beneath. The electrodes meeting acceptance criteria  $r_n^2 > 0.05$  were selected as features for classification for the face template. (B) As in (A), but for house stimuli from the training period. (C) Event-triggered broadband templates from the training period for face,  $\langle B_1(t') \rangle_F$ , and house,  $\langle B_1(t') \rangle_H$  stimuli, from the electrode noted with a green arrow in (A-B). (D) As in (C), but from the electrode noted with an orange arrow. (E) Projection of event-triggered face template from (C) into **testing data**: The top black trace shows a portion of the broadband time course from the electrode noted with a green arrow, during the testing period,  $B_1(t)$ . The  $\langle B_1(t') \rangle_F$  face template is shown in light blue at each stimulus time, irrespective of class, at event testing times  $\tau_p$ . The result of projecting the face template  $\langle B_1(t') \rangle_F$  to  $B_1(t)$  is shown in the green background trace,  $\Gamma_{1,F}^B(t)$ , with testing points at defined face stimulus times,  $\Gamma_{1,F}^B(p \rightarrow F)$ , shown with blue circles, and defined house stimulus times,  $\Gamma_{1,H}^B(p \rightarrow H)$ , shown with red circles. (F) As with (E), but for the orange-arrow electrode,  $B_2(t)$ , and using the house template from (D),  $\langle B_2(t') \rangle_H$ . (G) The subspace  $\Gamma_{1,F}^B$  vs  $\Gamma_{2,H}^B$ , is used to illustrate discrete classification approach. Here the back-projected training points  $\Gamma_{n,S}^B(q)$  are shown with dots (blue for  $q \rightarrow F$  and red for  $q \rightarrow H$ ), along with the testing feature points  $\Gamma_{n,S}^B(p)$  shown with circles. One may see that a simple decision line (purple) in this subspace would result in only 1 error.

doi:10.1371/journal.pcbi.1004660.g002

**Testing feature points for discrete classification**,  $\Gamma_{n,S}^V(p)$  and  $\Gamma_{n,S}^B(p)$ , were similarly obtained by **forward-projecting**  $\langle V_n(t') \rangle_S$  and  $\langle B_n(t') \rangle_S$  into the **testing period** for pre-defined times of face or house picture stimuli onset events,  $p$ , at times  $\tau_p$ . These results are illustrated in Fig 3.

**Projection of templates into continuous data stream (illustrated in Figs 4–6).** To quantify how well the averaged raw potential  $\langle V_n(t') \rangle_S$  is represented in the voltage time series of the testing data at time  $t$ , it is directly forward-projected onto the continuous time series at each

millisecond:  $\Gamma_{n,S}^V(t) = \sum_{t'=-199}^{400} \langle V_n(t') \rangle_S (V_n(t+t') - \overline{V_n^\tau(t)})$ , where  $\overline{V_n^\tau(t)}$  was obtained in the same fashion as above. The same projection is performed for the broadband template  $\langle B_n(t') \rangle_S$ , to obtain  $\Gamma_{n,S}^B(t)$ .

**Generation of a projection feature space.** The full feature space for classification, consisting of the union of projections of the stimulus triggered average raw potentials ( $V$ ) or broadband ( $B$ ) across all electrodes ( $n$ ), for faces ( $F$ ) and houses ( $H$ ) independently, is the combination of  $\Gamma_{n,F}^V$ ,  $\Gamma_{n,H}^V$ ,  $\Gamma_{n,F}^B$ , and  $\Gamma_{n,H}^B$ . For notational brevity, we can combine the notation to denote each feature as  $\Gamma_m$ , where  $m$  represents a unique combination of electrode  $n$ ,  $V$  or  $B$ , and  $F$  or  $H$ . Many of these features will not be particularly informative about when and how the brain is processing these visual stimuli, and reduce classification in the setting of a limited number of training measurements [35]. Therefore, features were individually downselected by independently assessing their squared cross-correlation between events of each stimulus type (e.g. face or house) and events drawn from the ISI during the training period, and rejecting those which fell beneath a pre-defined threshold  $r_m^2 < 0.05$ . For example, for projections of the face event-related feature,  $\Gamma_{n,F}$  ( $V$  /  $B$  label dropped here) we can denote the average of face stimuli as  $r_{n,F}^2 = \frac{(\overline{\Gamma_{n,F}(q=F)} - \overline{\Gamma_{n,F}(q=o)})^2}{\sigma_{n,Fo}^2} \frac{N_F * N_o}{N_F^2}$ , where  $\sigma_{n,Fo}$  is the standard deviation of the joint distribution for face and ISI events  $\Gamma_{n,F}(q = F, o)$ ,  $N_F$  is the number of face events,  $N_o$  is the number of

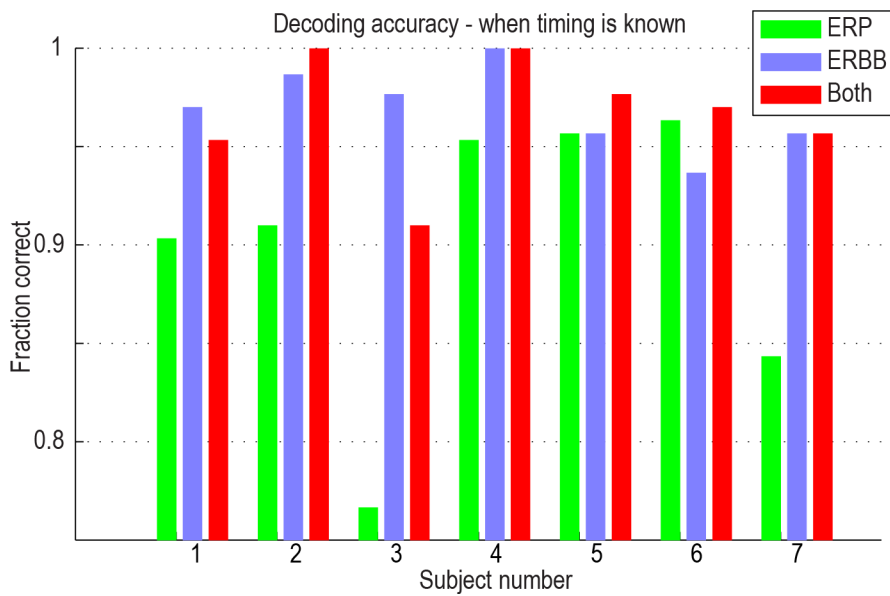


**Fig 3. Classification accuracy when the onset of a stimulus is known, using ERP, ERBB, or both template types.** In some subjects, 100% accuracy was reached. All accuracies were above 90% when both raw potential and broadband templates were used.

doi:10.1371/journal.pcbi.1004660.g003

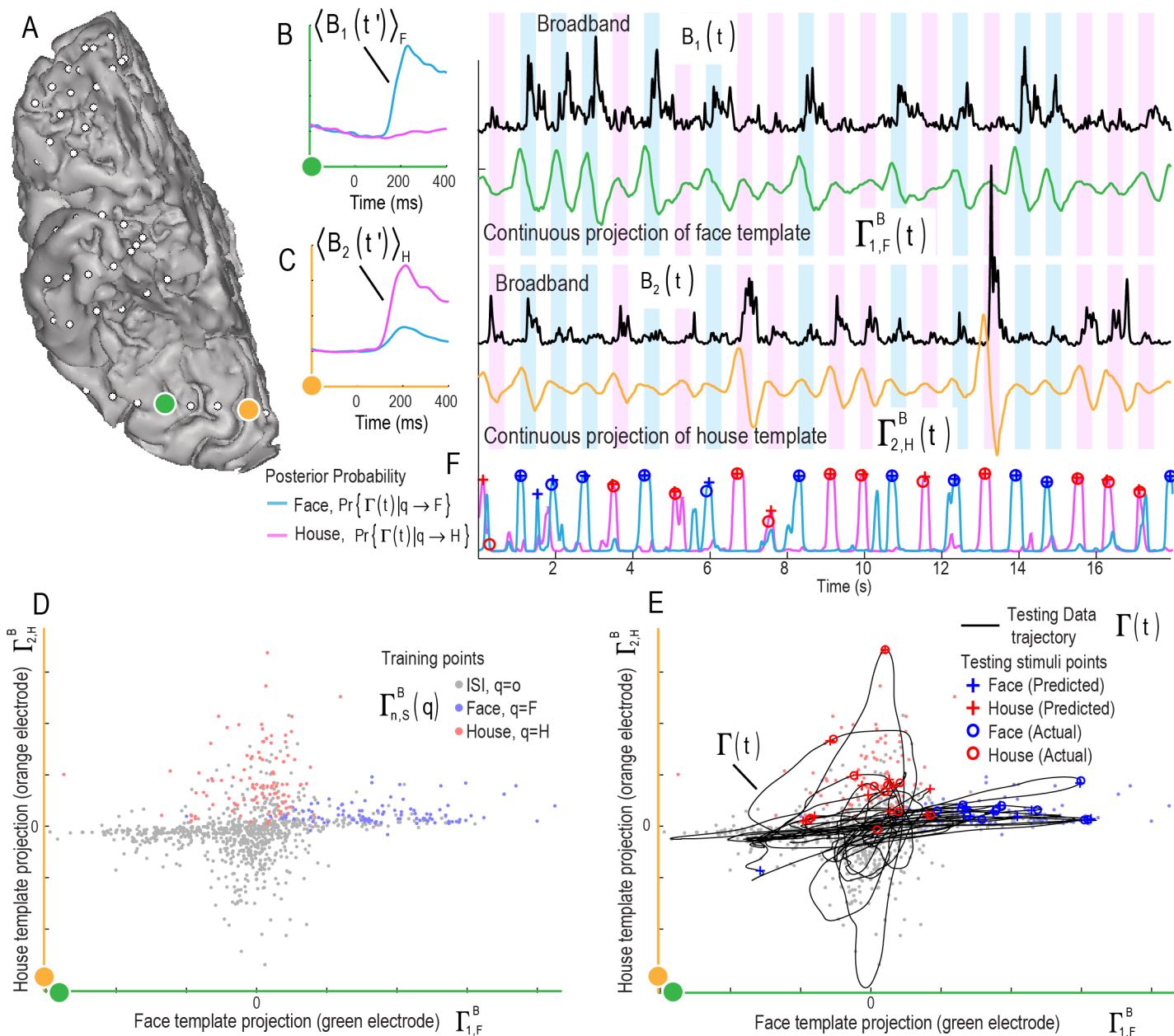


**Fig 4. Decoding stimulus class and onset time from a continuous data stream in single trials: Illustration of two electrodes and the continuous classifier using 2 broadband features (subject 2).** (A) Two cortical sites (3 cm from one another) on the fusiform (green) and lingual (orange) gyri are examined. (B) Broadband training templates from the green electrode for faces (blue,  $\langle B_1(t') \rangle_F$ ) and houses (pink,  $\langle B_1(t') \rangle_H$ ) are shown on the axes to the left. Testing time course of green electrode broadband spectral change,  $B_1(t)$ , is shown to the right in black, with the projection of the face template  $\langle B_1(t') \rangle_F$  into  $B_1(t)$  to produce  $\Gamma_{1,F}^B(t)$ , shown in the green trace beneath. (C) As in B, but for the orange electrode site, using projections of a house template  $\langle B_2(t') \rangle_H$  to produce  $\Gamma_{2,H}^B(t)$ . (D) The classification feature subspace is defined by back-projection of the templates on the left in (B-C), to obtain training points  $\Gamma_{n,S}^B(q)$  for face, house, and ISI events at training times  $\tau_q$  shown. (E) In order to illustrate the multi-dimensional trajectory of the brain state that emerges when different channels and features are brought into a common space, the 2D trace of  $\Gamma_{1,F}^B(t)$  from the green electrode (B) versus  $\Gamma_{2,H}^B(t)$  from the orange electrode (C), are shown in black in the same subspace as D. The predicted onsets for face (blue) and house (red) stimuli are shown as plus symbols while actual onsets are shown as open circles. Note that the classifier was applied to the entire broadband feature space, not just this 2D subspace. (F) The trajectory of the face onset posterior probability from the classifier  $\Pr\{\Gamma(t)|q \rightarrow F\}$  (blue) is shown alongside  $\Pr\{\Gamma(t)|q \rightarrow H\}$  (pink), with predicted (plus symbols) and actual (open circles) times shown.

doi:10.1371/journal.pcbi.1004660.g004

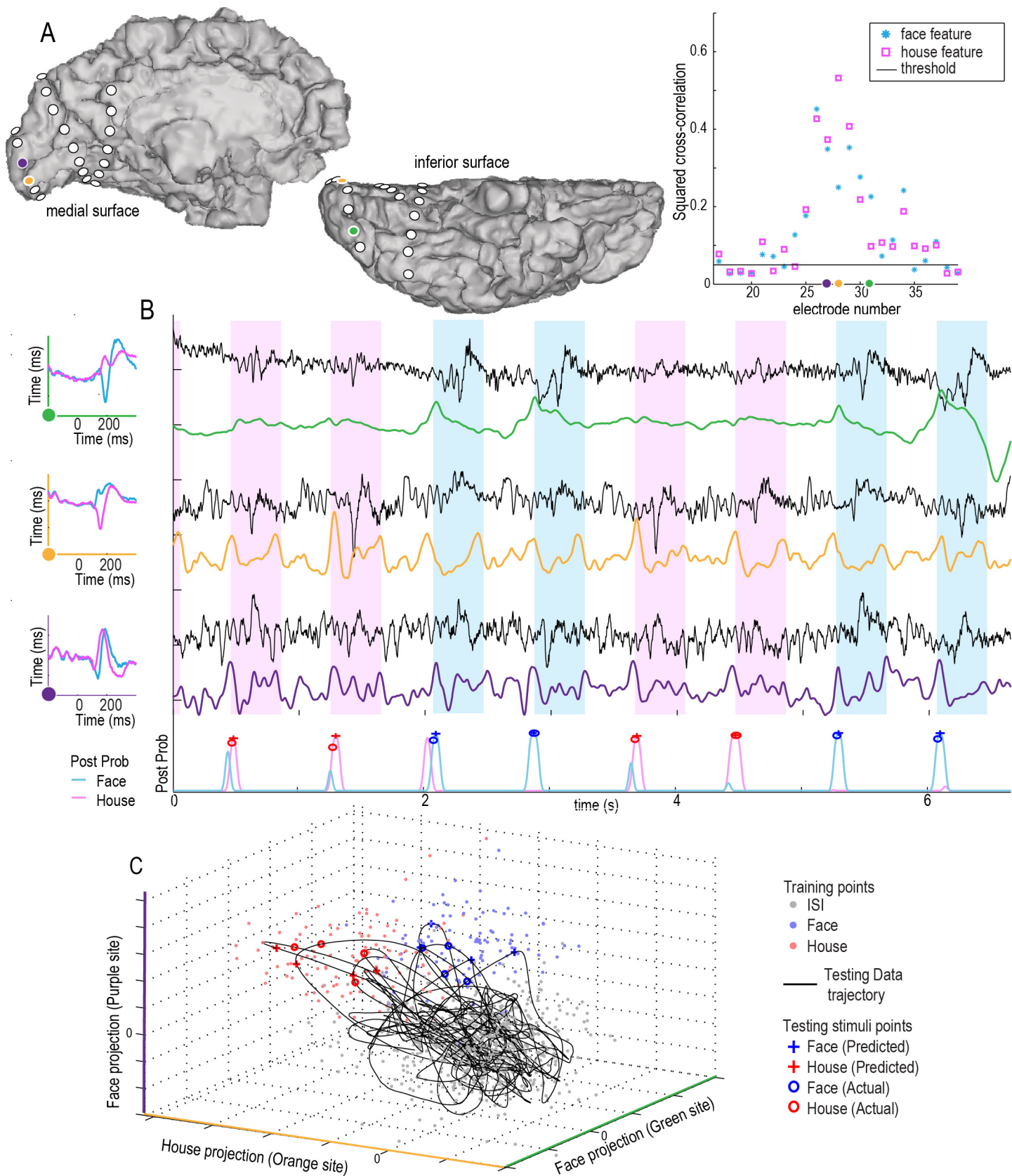


**Fig 5. Decoding the single trial stimulus class and onset time from a continuous data stream using ERP: Illustration of three electrodes and the continuous classifier using 3 ERP-templates-to-voltage-timeseries projections (subject 4).** (A) Three cortical sites are shown for illustration (purple, orange, and green). The axes on the right show the  $r_{n,F}^2$  (blue asterisk,  $r^2$  of faces-vs-ISI) and  $r_{n,H}^2$  (pink box,  $r^2$  of houses-vs-ISI) of ERP-voltage training projections show that these purple/orange/green sites are highly selective for faces or houses during the **training period** (from the 1<sup>st</sup> cross-fold). Features falling below the black line were not used for decoding. (B) Averaged face and house ERPs,  $\langle V_n(t') \rangle_F$  &  $\langle V_n(t') \rangle_H$ , from each site are shown on the left axes. These are projected into the raw voltage traces from the **testing period** ( $V_n(t)$ , black) to obtain continuous projection weight traces ( $\Gamma_{n,F/H}^V$ ; green–face projection from green electrode, orange–house projection from orange electrode, and purple–face projection purple electrode). These traces are fed into a feature space and classified continuously to obtain posterior probability of a face,  $\Pr\{\Gamma(t)|q \rightarrow F\}$  (blue), or house stimulus,  $\Pr\{\Gamma(t)|q \rightarrow H\}$  (pink) (bottom plot). (C) A 3-dimensional subspace (from the sites in A and B) is illustrated, with training points from the training period shown with dots, and the subspace trajectory of the brain state,  $\Gamma(t)$ , shown with a black line. Predicted and actual timing and type of stimulus are shown along this trajectory.

doi:10.1371/journal.pcbi.1004660.g005

ISI events, and  $N_{Fo} = N_F + N_o$ . In this study, we consider feature spaces consisting of projections of all types (e.g. ERP and ERBB together), and also selectively assess  $B(t)$  and  $V(t)$  independently. Example feature (sub)spaces are illustrated in Figs 2G and 4D and 4E and 5C and 6H–6L.

**Classifier type and relation to feature space.** We begin with the feature set of training points ( $q$ , drawn from only the training period),  $\Gamma_m(q)$ , where each  $m$  is a dimension in the feature space, and represents a particular combination of electrode, broadband or raw potential time series, and face or house template. For the sake of simplicity, Fisher linear discriminant analysis (LDA) was used for classification [36]. This characterizes the full distribution and the training period sub-distributions  $\Gamma_m(q \rightarrow F)$ ,  $\Gamma_m(q \rightarrow H)$ ,  $\Gamma_m(q \rightarrow o)$ , by their means and covariances only (i.e., as if they are normally distributed). LDA assumes that the covariances of the sub-distributions are the same. Given these training distributions, data from the testing set can be assigned a posterior probability of belonging to each distribution. While we used simple LDA, one could, in principle, apply more sophisticated kernel-based or non-linear methods. Our choice of LDA was meant to simplify interpretation of our approach, which is centered on the generation of “projection feature spaces”, and provide a clear demonstration of how one may decode a continuous datastream spontaneously, rather than exploring the library of existing machine learning and classifier techniques, which is deferred to future study.

**Classification of discrete events with known onset time (Fig 3).** We began with the case where we identify the timing of testing visual stimuli, and attempt to classify whether a face or a house picture was shown. Only the face and house training point distributions (e.g.  $\Gamma_m(q \rightarrow F)$  and  $\Gamma_m(q \rightarrow H)$ ) were used to train the classifier for this discrete case. For each testing point,  $p$ , the assigned class was whichever posterior probability  $\Pr\{\Gamma(p)|q \rightarrow F\}$ , or  $\Pr\{\Gamma(p)|q \rightarrow H\}$ , was higher.

**Spontaneous decoding of the continuous datastream (Fig 7).** For the prediction of type and timing of visual stimulus from continuous signal, we trained the classifier using the face ( $\Gamma_m(q \rightarrow F)$ ), house ( $\Gamma_m(q \rightarrow H)$ ), and ISI ( $\Gamma_m(q \rightarrow o)$ ), training point distributions. Then, the LDA posterior probability that a face or house stimulus has been shown at any point in time can be measured from the testing data at each millisecond  $t$  as  $\Pr\{\Gamma(t)|q \rightarrow F\}$  or  $\Pr\{\Gamma(t)|q \rightarrow H\}$ . We then smooth each of these posterior probabilities with a  $\sigma = 80$ ms Gaussian filter, for well-behaved estimation of local maxima. From this, we assign predicted times for stimuli onset as follows: The posterior probability must be a local maximum, with value  $>0.51$ . There must be at least 320 ms between any point and the nearest assigned point (of either stimulus type—the larger posterior probability ‘wins’). A guess is considered correct if it lies within 160ms of an event. The probability of the null case,  $\Pr\{\Gamma(t)|q \rightarrow o\} = 1 - \Pr\{\Gamma(t)|q \rightarrow F\} - \Pr\{\Gamma(t)|q \rightarrow H\}$ , is  $>0.50$  at all other times, signifying that a picture has not just been shown.

While no information was given about the frequency of the stimuli, it was assumed that visual events were neuronally and behaviorally separable and a minimum difference of 320 ms was used. We picked 320ms as the “collision time” because we expect the neuronal response to

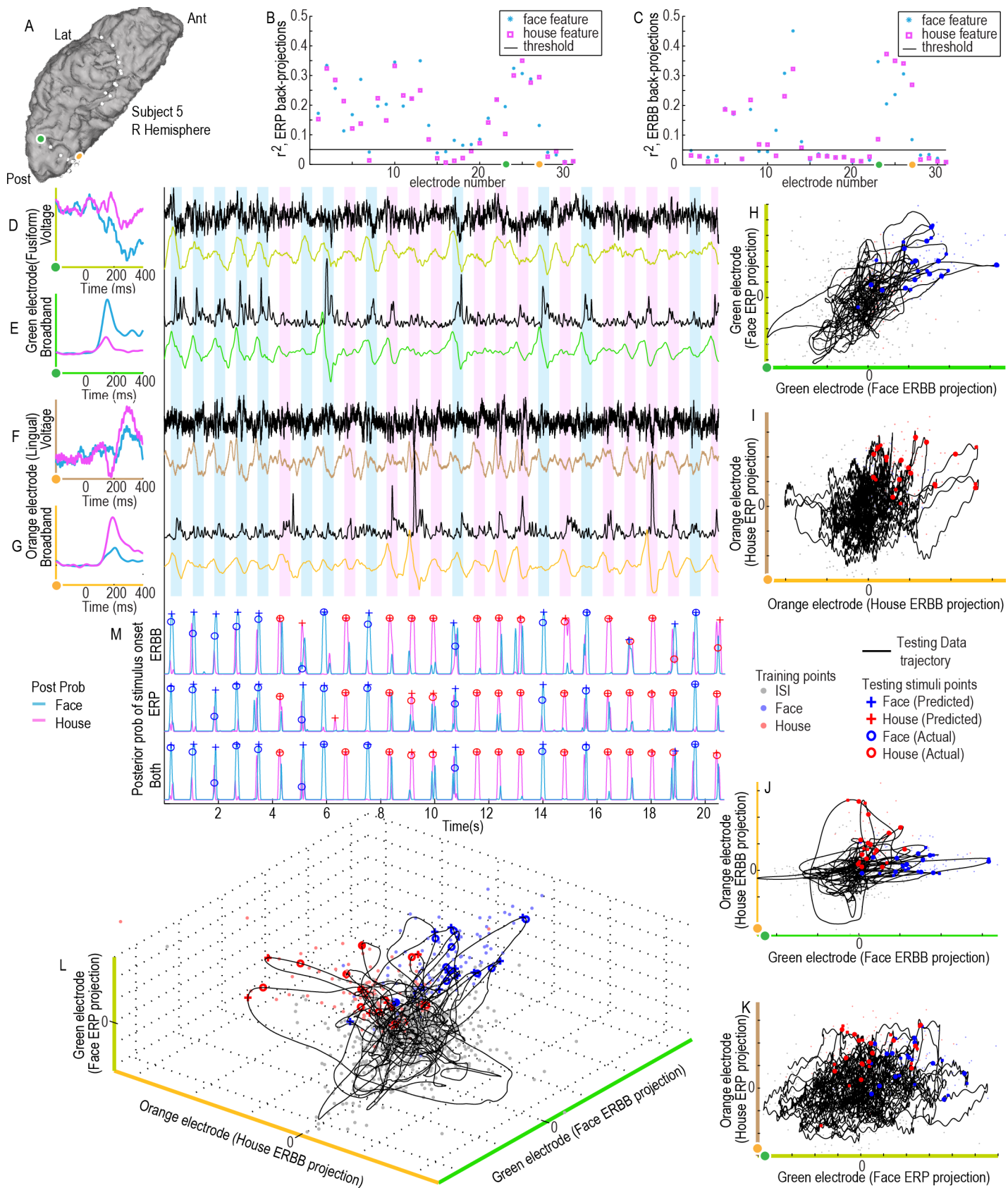


**Fig 6. A combined ERBB-broadband and ERP-voltage projection feature space for classification (subject 5).** (A) Two cortical sites (orange and green dots) are examined. (B) The axes show the  $r_{n,F}^2$  (blue asterisk) and  $r_{n,H}^2$  (pink box) for **ERP-voltage training** projections show that these orange and green sites are highly selective during the training period (from first cross-fold). (C)  $r_n^2$  for **ERBB-Broadband training** projections. (D) Averaged face and house ERP templates from the green site are shown on the left axes (olive green). The face-ERP templates are projected into the raw voltage trace (black) to obtain continuous a projection weight trace (olive green trace). (E) As in (D), but for ERBB-broadband templates in the green electrode site (neon green). (F&G) As in (D&E), except for the orange electrode site in (A), using house ERP (brown) and ERBB (burned orange) templates. (H) Green electrode, face ERP vs ERBB subspace projections. (I) Orange electrode house ERP vs ERBB subspace projections. (J) ERBB projection subspace (orange-electrode house-template projection vs green-electrode face-template projection). (K) As in (J), for ERP projection subspace. (L) A 3-d subspace projection (features from D, E,G). (M) Posterior probability of a face,  $\Pr[\Gamma_m(t)|q \rightarrow F]$  (blue), or house stimulus,  $\Pr[\Gamma_m(t)|q \rightarrow F]$  (pink), having been presented (where  $m \rightarrow$  ERP, ERBB or both features for the projection space).

doi:10.1371/journal.pcbi.1004660.g006

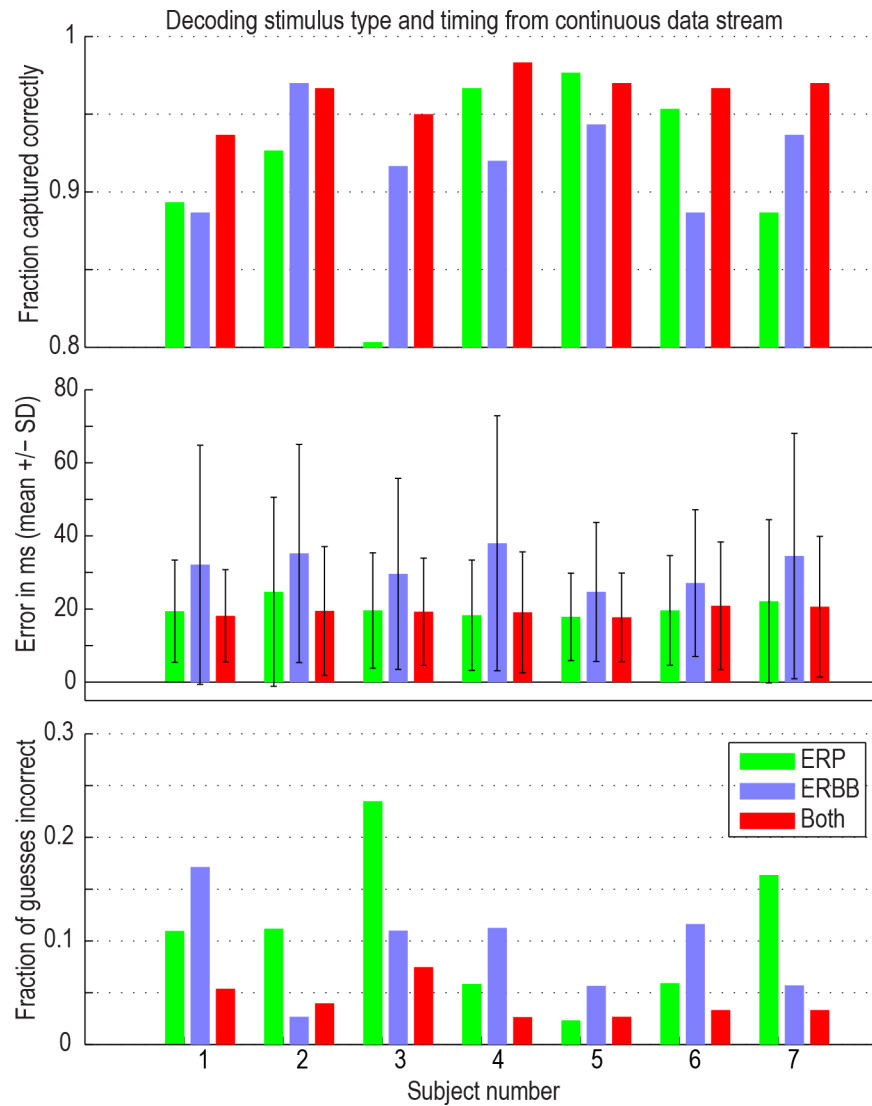


**Fig 7. Classification accuracy for decoding stimulus class and onset in a continuous data stream.** When both features were used (red bars), approximately 96% of all stimuli were captured correctly in every subject, with 15–20 ms error. An average of 4% of predictions using both features were incorrect (i.e., predicted stimuli at the wrong time, or as the wrong class). One should not confuse the fraction of guesses incorrect with the fraction of stimuli that were not captured (the bars on the top and bottom axes do not sum to 1—it is a coincidence that also 4% of stimuli were missed).

doi:10.1371/journal.pcbi.1004660.g007

take approximately that long [37], it makes for a random hit rate of 20% (e.g. 2.5 guesses per 800ms stimulus-to-stimulus interval, with 2 stimulus classes), and it roughly correlates with the mean broadband latencies-to-peak across single trials in these brain areas, which were found in other studies to be  $269 \pm 52$ ms for face-selective ventral temporal sites and  $299 \pm 66$ ms for house-selective sites [13]. This threshold for the classifier is also based in the following known aspects of the time scales of neuronal responses and face perception. First, when visual stimuli are shown in rapid order, it becomes impossible to visually distinguish each stimulus at specific rates for different stimulus classes [38,39]. For face perception this behavioral rate lies around 5–10Hz [40]. At faster rates, backward masking and temporal integration become issues. Second, the duration of a neuronal response in higher order visual areas is around 300 ms [41]. When stimuli are presented at faster rates than 300 ms each, neuronal responses from these brain areas would be expected start overlapping. Supporting information (S1 Fig) empirically shows that this choice of 320ms does not inform the classifier about frequency of stimuli shown.

In the case of spontaneous decoding of the continuous timeseries, if one were to make random guesses for events at the maximum permissible temporal density of guesses (using the rules we picked in the methodology), each guess would have a 20% chance of being correct, and 50% of stimuli would be deemed “captured”, with an 80% false positive rate, and an average temporal error of 80ms. Instead, 96% of stimuli (300 per subject) were captured, with a 4% false positive rate, and an average temporal error of 20ms.

When examining timecourses of the projections ( $\Gamma_n(t)$ ), as well as the resulting posterior probabilities ( $\Pr\{\Gamma(t)|q\}$ ), it is important to keep in mind that the templates ( $\langle V_n(t') \rangle_S$  and  $\langle B_n(t') \rangle_S$ ) contain temporal information up to ~400ms later (illustrated in Figs 2–6). The local maximum of the posterior probability is assumed to be roughly the time at **which the templates align** with the average response in such a way that the average response would be at the time of stimulus presentation. The portion of the signal that contributes the most to the cross-correlation is likely to be in the 150–350ms following the timepoint,  $t$  (based upon visual inspection of the templates and raw timecourses in Figs 1–6, as well as measured latencies in [13]).

## Results

ECOG signals were measured in seven subjects from electrodes implanted on the inferior temporal visual areas for the purpose of epilepsy monitoring. Subjects were presented with pictures of faces and houses (similar to those in Fig 1). We attempted to spontaneously identify the timing of face and house visual stimuli.

### Signal features for decoding: Event-related broadband (ERBB) and event-related potential (ERP)

To test whether the ERBB and ERP provide useful information to decode whether, when and which class of stimulus was presented, we extracted the ERBB and ERP for all electrodes. Some electrodes show a classical face-specific N200 response [13–15]. Other electrodes show face-specific ERPs with very different shapes (Fig 1).

### Decoding the stimulus class in single trials when the onset of a stimulus is known

We first investigated whether the stimulus class could be decoded in single trials when the onset of the stimulus is given. We calculated template ERBB and ERP responses from training

data, which consisted of 2/3 of the recorded data (two experimental runs). The test data (for the classifier) consisted of the other 1/3 (the remaining experimental run; i.e., 3-fold cross validation, or “leave-one-run-out” cross-validation). [Fig 2](#) shows examples of the template ERBB responses for a face- and a house-specific site. Even in a two-dimensional subspace of the full feature space, a simple line serves as a good classification boundary between the two classes of stimuli ([Fig 2G](#)).

Using either the ERP or the ERBB feature, stimuli could be robustly and reliably categorized in all cases. The average prediction accuracy using the ERBB alone was 97% across all 7 subjects, while using the ERP alone, it was 90% ([Fig 3](#)). Using a combination of the two features, 97% of stimuli could accurately be classified as face or house. It is important to note that, in subjects 1 and 3, the addition of the ERP feature actually resulted in a decrease in classification accuracy, when compared with the ERBB alone, and subject 7 shows no change. This is because of what is known as the “bias-variance tradeoff” [42,43]. For a finite number of datapoints in a training set, the inclusion of features with higher amounts of noise (ERP features in this case) can hurt overall classification. The classifier overfits noise in the mediocre features (ERP), at the expense of a tight fit to high-yield (lower noise) features (e.g. ERBB), while simultaneously expanding the size of the feature space.

### Spontaneous decoding of stimulus class and onset from a continuous cortical data stream

Figs [2](#) and [3](#) demonstrate that our analyses can accurately determine the stimulus class when given the timing of stimulus presentation. However, this type of decoding has been employed before in other experimental settings, albeit with less accuracy [20–22]. The more interesting technical question is: Can one spontaneously determine both the class and the onset of the stimuli from a continuous stream of ECoG signal features?

Our approach to the continuous decoding problem is illustrated in Figs [4](#)–[6](#), where template responses from a training period were applied to a period of testing data. The result of plotting the projection timeseries trajectory in a 2-dimensional subspace,  $\Gamma^B(t)$ , can be seen alongside training points  $\Gamma_{n,S}^B(q)$  in [Fig 4](#). Even in this 2-dimensional subspace projection, the furthest excursions of  $\Gamma^B(t)$  into the face or house training clouds,  $\Gamma_{n,S}^B(q)$ , correlate with the times of predicted stimulus onset. [Fig 5](#) shows an example similar to that in [Fig 4](#), but for the ERP feature. [Fig 6](#) shows an example of the synthesis between ERP and ERBB features when used together.

A combination between ERP and ERBB projections can be used to predict the onset timing and class of stimuli more accurately than either independently. The spontaneous classification of onset time and stimulus class was robust: 92% of stimuli were captured using the ERBB, 92% when using the ERP, and 96% of all stimuli were captured spontaneously when using a combination of both ERP and ERBB ([Fig 7](#), top row). Furthermore, timing of stimulus onset could be predicted with approximately 20ms error when the ERP or a combination between the ERP and ERBB was used ([Fig 7](#), middle row). The portion of incorrect predictions (e.g. false positive rate) was smallest (4%) when we used a combination of both the ERP and ERBB (i.e., predicted stimuli occurred at >160ms from stimulus onset, or as the wrong class; [Fig 7](#), bottom row).

In order to evaluate whether using both features together (ERP and ERBB) was significantly better than either independently, the labels of mean values (ERP vs ERBB vs ERP+ERBB) were randomly reshuffled (within each subject)  $10^4$  times to obtain a surrogate distribution of difference in means averaged across all subjects. The 96% of events captured using both features was significantly greater than the 92% when using either independently ( $p = 0.0015$ ). The timing error for correct predictions was not significantly different for both features (19ms) vs ERP

(20ms,  $p = 0.17$ ), but was significantly better than ERBB alone (32ms,  $p < 0.0001$ ). The false positive rate using both features (0.04) was significantly less than either independently (ERP 0.11; ERBB 0.09;  $p = 0.0012$ ). The fact that the overall best prediction performance was reached by a combination of ERBB and ERP suggests that these two cortical features convey complementary information about a subject's perceptual state.

Note that our 20ms estimate of the temporal fidelity of the signals may actually be an underestimate. There may be instrumentation temporal error introduced due to frame-jitter on the refresh rate of the amplifiers, sample jitter during alignment to the stimulus, and/or the granularity of sample block size of the signals imported to BCI2000 program [30]. Furthermore, there are known variations in the magnitude and timing broadband responses that are related to semantic properties (such as novelty [13]), that are disregarded in this manuscript.

We designate this technique as “Spontaneous decoding” of the ECoG datastream. Our technique processes the data, without foreknowledge of the frequency of external stimuli, nor their timing, nor their content. It then produces predictions about the occurrence, timing, and content of external stimuli, based upon a simple set of internal rules. “Spontaneous” is defined as [44]: “performed or occurring as a result of a sudden inner impulse or inclination and without premeditation or external stimulus”, and so we feel that this term is the most specific way to describe this analysis approach. While “endogenous” or “intrinsic” decoding might also have been chosen, since these are used to describe internal brain states (which is an aspect of what we are actually decoding), we chose not to use them—we feel that these terms convey assumptions about the role of the temporal lobe which have yet to be proven.

## Discussion

In human experience, environmental stimuli arrive continuously, producing a sequentially evolving perceptual state. It has remained unknown whether the brain surface electrical potential has sufficient spatiotemporal fidelity to capture this dynamically changing perceptual state. Our results demonstrate that a sparse sample of the cortical surface potential contains sufficient information to reliably predict *whether* and *when* a particular stimulus occurred, with approximately the fidelity of conscious perception. It has also remained unknown whether the meso-scale neurophysiologies of event-related potentials and broadband spectral changes reflect the same information.

Previous studies aimed at decoding perception have all pre-defined the onset time of each stimulus [6,20–22,45,46]. In the first-stage of our analysis, we performed this type of classification using pre-defined onset time, with 97% accuracy (Figs 2 and 3). Similar prior studies attained representative peak accuracies of 72% with MEG/fMRI [22], 89% with EEG [20], and 94% with MEG [21]. However, real-world perception rarely occurs at pre-defined times, and approaches to decoding perceptual experience should be extracted spontaneously from continuous cortical recordings.

We have developed a technique to do just this, applying a novel template projection technique that enabled us to capture some aspects of the neural response that have previously been difficult or impossible to capture. First, the ERP in face-selective regions in the fusiform gyrus is classically associated with a negative peak at ~200ms (“N200”). Our data show that the actual shape of face-selective fusiform ERPs can vary widely, even at fusiform sites 1 cm from one another (Fig 1). The template projection technique captures these diverse response patterns, allowing them to be exploited for classification of perceptual state. Second, broadband responses show variability in the pattern of response in every individual trial. The template projection method relies on a superposition of the single trial characteristic shape and a probability density function for modeling different shapes, offering a robust prediction of perceptual

state in spite of the variability across single trials. Examination of the features separately demonstrated that broadband changes are more robust and reliable reflections of perceptual content than raw-voltage changes, but that projection of ERP into raw voltage changes produces sharper temporal precision. Together, these two measures complement one another, providing independent information that results in more accurate and temporally precise prediction of the perceptual state than either measure on its' own.

Our decoding fidelity approaches that of conscious thought, correctly capturing 96% of all stimuli from a sparsely-sampled stream of cortical potentials. The missed 4% (as well as the <5% false positive rate) approaches what might be expected for rates of inattention by hospital patients viewing multiple stimuli each second (note that random guessing at the maximum rate in this spontaneous decoding would result in a 20% chance of each guess being correct, and 50% of stimuli deemed “captured”, with an 80% false positive rate). A temporal precision of ~20ms (Fig 7, middle row) is of the same order as the post-retinal temporal granularity of the visual system [47]. These ECoG measurements show that some electrodes in early visual cortex already display some stimulus-selective responses (e.g., Fig 5, purple site). This agrees with observations that fast eye movements can be made just based upon the Fourier spectrum of the images of different classes [48], and that people saccade towards a scene containing an animal or face within 140 ms [49,50]. By demonstrating that object categories can be decoded from a continuous image stream with accuracies matching expected human behavior (e.g. attentional lapses expected at a rate of approximately 5% in a task of this type [51]), our study lays the groundwork for capturing human perceptual states in a natural environment.

Although we applied this template-projection technique to prediction, the framework may be used in a wide variety of experimental settings. ERPs from adjacent cortical regions may be highly polymorphic, complicating cross-comparison of timing and magnitude effects. In this projection space, however, trial-to-trial ERP variations from different cortical sites may be compared directly, opening a new family of analyses that might be applied to cognitive settings, where image content and context are experimentally manipulated on single trials. Similarly, one might optimize the differential strengths of each feature, such as broadband for magnitude of response and ERP for timing of response, comparing these to stimulus properties to learn about subtleties of functional specialization in each brain region.

An important feature of this template projection approach is that it provides a robust, continuous, measure that is a summary statistic for how well the brain state at every point in time reflects the expected response (e.g. as if a perceptual event or action had occurred at that time—note that the shape of the expected physiological response, however idiosyncratic, is built into the method). This could be extremely useful in settings where the cortical dynamics and latency differ by region, yet a global behavior of a distributed visual [52], auditory [53,54], motor [55], or other network must be characterized. In emerging work, this technique is implemented in a different way, to generate broadband ECoG templates from a low-noise localizer task, and apply them to a visual discrimination task at the perceptual threshold, quantifying single trial variation in cortical physiology (neuronal response magnitude and timing) [56].

Our results beg the question: What is the underlying neural basis for the increased accuracies obtained by combining ERPs with broadband activity? A direct connection between neuronal population firing rate and broadband ECoG spectral change has been established with experimental and modeling work [11,23,24]. Each clinical ECoG electrode averages over approximately  $5 \times 10^6$  neurons in the cortex beneath. Careful experimentation has shown that the broadband changes follow a power law in the power spectral density, implying that it reflects *asynchronous* spiking elements in the underlying population of neurons. The broadband measure may be loosely thought of as a real-time summation of this population's firing raster (i.e., intrinsically averaged across the population of neurons). Increases in spike

transmission within neurons in the population add in quadrature (e.g., proportional to the square root of the number of spikes), appearing as a “speeding up” of a random walk in the electrical potential time series, *are difficult to see when looking at the raw potential*, but apparent as broadband,  $P \sim 1/f^z$  power-law, changes when inspecting in the frequency domain [24]. Recent work has shown that, in these data, the broadband timing is subtle enough to capture variational effects at the order of ~50ms due to context-dependent processing, such as sequential novelty [13].

Synchronized inputs, by contrast, add linearly and *can be easily seen in the raw tracing of the electrical potential*. Even if the synchronization is relatively weak, averaging across the neural population augments the synchronized portion, while the other aspects, such as broadband spectral change, are relatively diminished. Event-locked inputs, from subcortical nuclei, or other cortical regions, can trigger a synchronized physiologic cascade, evident at the macro-scale as an ERP. It remains unclear whether the polyphasic ERP is a result of interplay between coordinated excitatory pyramidal neuron depolarization followed by interneuronal lateral inhibition, or whether it results from synaptic integration followed by characteristic depolarization and repolarization of cortical laminar dipoles [57]. The polymorphic nature of different ERPs from adjacent cortical regions may (perhaps) then relate to different pyramidal neuron morphologies, different milieus of neuronal subtypes, or different laminar organization; our projection technique unfolds these polymorphic ERPs into a common space for comparison. In this light, the improved decoding accuracy may be the result of multi-location timing information conveyed by ERP during the initial feed-forward wave of neural activation [58], complemented by the broadband response reflecting subsequent local recurrent and longer-range cortico-cortical processing of the visual stimulus.

## Supporting Information

**S1 Table. Participant characteristics, and number of selected electrodes by  $r^2 < 0.05$  criteria (from first fold only).**

(PDF)

**S2 Table. Correct classifications, when the timing of events is pre-designated.** Sorted by stimulus type (note that each number is out of a possible 150 correct).

(PDF)

**S3 Table. Errors for Spontaneous Predictions.**

(PDF)

**S1 Text. Power spectral analysis.**

(PDF)

**S2 Text. Decoupling the cortical spectrum.**

(PDF)

**S1 Fig. Choice of collision time does not inform classifier about timing of events.** Number of false predictions as a function of the choice of maximum distance between predicted event times (Collision time), for classification using both ERP and ERBB. The monotonic decay form and lack of “dips” or “peaks” shows that the collision time chosen did not inform the classifier about timing of stimuli. Of note, subject 5, who had the most early visual electrodes, was unaffected by even very low collision times. The number of events correctly predicted was the same for every choice of collision time, so those data are not shown.

(TIF)

## Acknowledgments

We are grateful to the patients and staff at Harborview Hospital in Seattle. Discussions with Kalanit Grill-Spector, Nick Ramsey, David Heeger, Bharathi Jagadeesh, Nathan Wittoft, and Brian Wandell were extremely helpful. Sara Webb created the stimuli and generously shared them with us.

## Author Contributions

Conceived and designed the experiments: KJM JGO RP NR. Performed the experiments: KJM JGO. Analyzed the data: KJM DH. Contributed reagents/materials/analysis tools: KJM. Wrote the paper: KJM GS DH JGO RP NR.

## References

1. Kanwisher N, McDermott J, Chun MM (1997) The fusiform face area: a module in human extrastriate cortex specialized for face perception. *The Journal of neuroscience: the official journal of the Society for Neuroscience* 17: 4302–4311.
2. Epstein R, Kanwisher N (1998) A cortical representation of the local visual environment. *Nature* 392: 598–601. PMID: [9560155](#)
3. Aguirre GK, Zarahn E, D'Esposito M (1998) An area within human ventral cortex sensitive to "building" stimuli: evidence and implications. *Neuron* 21: 373–383. PMID: [9728918](#)
4. Puce A, Allison T, Gore JC, McCarthy G (1995) Face-sensitive regions in human extrastriate cortex studied by functional MRI. *Journal of neurophysiology* 74: 1192–1199. PMID: [7500143](#)
5. Kreiman G, Koch C, Fried I (2000) Category-specific visual responses of single neurons in the human medial temporal lobe. *Nat Neurosci* 3: 946–953. PMID: [10966627](#)
6. Kiani R, Esteky H, Mirpour K, Tanaka K (2007) Object category structure in response patterns of neuronal population in monkey inferior temporal cortex. *J Neurophysiol* 97: 4296–4309. PMID: [17428910](#)
7. Ghuman AS, Brunet NM, Li Y, Konecky RO, Pyles JA, et al. (2014) Dynamic encoding of face information in the human fusiform gyrus. *Nat Commun* 5: 5672. doi: [10.1038/ncomms6672](#) PMID: [25482825](#)
8. Privman E, Fisch L, Neufeld MY, Kramer U, Kipervasser S, et al. (2011) Antagonistic relationship between gamma power and visual evoked potentials revealed in human visual cortex. *Cereb Cortex* 21: 616–624. doi: [10.1093/cercor/bhq128](#) PMID: [20624838](#)
9. Vidal JR, Ossandon T, Jerbi K, Dalal SS, Minotti L, et al. (2010) Category-Specific Visual Responses: An Intracranial Study Comparing Gamma, Beta, Alpha, and ERP Response Selectivity. *Front Hum Neurosci* 4: 195. doi: [10.3389/fnhum.2010.00195](#) PMID: [21267419](#)
10. Kadipasaoglu CM, Baboyan VG, Conner CR, Chen G, Saad ZS, et al. (2014) Surface-based mixed effects multilevel analysis of grouped human electrocorticography. *Neuroimage* 101: 215–224. doi: [10.1016/j.neuroimage.2014.07.006](#) PMID: [25019677](#)
11. Miller KJ, Zanos S, Fetz EE, den Nijs M, Ojemann JG (2009) Decoupling the Cortical Power Spectrum Reveals Real-Time Representation of Individual Finger Movements in Humans. *Journal of Neuroscience* 29: 3132. doi: [10.1523/JNEUROSCI.5506-08.2009](#) PMID: [19279250](#)
12. Miller KJ, Honey CJ, Hermes D, Rao RP, denNijs M, et al. (2014) Broadband changes in the cortical surface potential track activation of functionally diverse neuronal populations. *Neuroimage* 85 Pt 2: 711–720.
13. Miller KJ, Hermes D, Wittoft N, Rao RP, Ojemann JG (2015) The physiology of perception in human temporal lobe is specialized for contextual novelty. *J Neurophysiol* 114: 256–263. doi: [10.1152/jn.00131.2015](#) PMID: [25972581](#)
14. Allison T, Ginter H, McCarthy G, Nobre AC, Puce A, et al. (1994) Face recognition in human extrastriate cortex. *Journal of neurophysiology* 71: 821–825. PMID: [8176446](#)
15. Allison T, McCarthy G, Nobre A, Puce A, Belger A (1994) Human extrastriate visual cortex and the perception of faces, words, numbers, and colors. *Cerebral cortex* 4: 544–554. PMID: [7833655](#)
16. Huettel SA, McKeown MJ, Song AW, Hart S, Spencer DD, et al. (2004) Linking hemodynamic and electrophysiological measures of brain activity: evidence from functional MRI and intracranial field potentials. *Cerebral cortex* 14: 165–173. PMID: [14704213](#)
17. Engell AD, Huettel S, McCarthy G (2012) The fMRI BOLD signal tracks electrophysiological spectral perturbations, not event-related potentials. *NeuroImage* 59: 2600–2606. doi: [10.1016/j.neuroimage.2011.08.079](#) PMID: [21925278](#)

18. Jacques C, Witthoft N, Weiner KS, Foster BL, Rangarajan V, et al. (2015) Corresponding ECoG and fMRI category-selective signals in Human ventral temporal cortex. *Neuropsychologia*.
19. Engell AD, McCarthy G (2011) The Relationship of Gamma Oscillations and Face-Specific ERPs Recorded Subdurally from Occipitotemporal Cortex. *Cerebral cortex* 21: 1213–1221. doi: [10.1093/cercor/bhq206](https://doi.org/10.1093/cercor/bhq206) PMID: [20961973](#)
20. Simanova I, van Gerven M, Oostenveld R, Hagoort P (2010) Identifying object categories from event-related EEG: toward decoding of conceptual representations. *PloS one* 5: e14465. doi: [10.1371/journal.pone.0014465](https://doi.org/10.1371/journal.pone.0014465) PMID: [21209937](#)
21. van de Nieuwenhuijzen ME, Backus AR, Bahramisharif A, Doeller CF, Jensen O, et al. (2013) MEG-based decoding of the spatiotemporal dynamics of visual category perception. *NeuroImage* 83: 1063–1073. doi: [10.1016/j.neuroimage.2013.07.075](https://doi.org/10.1016/j.neuroimage.2013.07.075) PMID: [23927900](#)
22. Cichy RM, Pantazis D, Oliva A (2014) Resolving human object recognition in space and time. *Nat Neurosci* 17: 455–462. doi: [10.1038/nn.3635](https://doi.org/10.1038/nn.3635) PMID: [24464044](#)
23. Manning JR, Jacobs J, Fried I, Kahana MJ (2009) Broadband shifts in local field potential power spectra are correlated with single-neuron spiking in humans. *Journal of Neuroscience* 29: 13613. doi: [10.1523/JNEUROSCI.2041-09.2009](https://doi.org/10.1523/JNEUROSCI.2041-09.2009) PMID: [19864573](#)
24. Miller KJ, Sorensen LB, Ojemann JG, den Nijs M (2009) Power-law scaling in the brain surface electric potential. *PLoS Comput Biol* 5: e1000609. doi: [10.1371/journal.pcbi.1000609](https://doi.org/10.1371/journal.pcbi.1000609) PMID: [20019800](#)
25. Ashburner J, Friston KJ (2005) Unified segmentation. *NeuroImage* 26: 839–851. PMID: [15955494](#)
26. Wells WM 3rd, Viola P, Atsumi H, Nakajima S, Kikinis R (1996) Multi-modal volume registration by maximization of mutual information. *Med Image Anal* 1: 35–51. PMID: [9873920](#)
27. Hermes D, Miller KJ, Noordmans HJ, Vansteensel MJ, Ramsey NF (2010) Automated electrocorticographic electrode localization on individually rendered brain surfaces. *Journal of neuroscience methods* 185: 293–298. doi: [10.1016/j.jneumeth.2009.10.005](https://doi.org/10.1016/j.jneumeth.2009.10.005) PMID: [19836416](#)
28. Dale AM, Fischl B, Sereno MI (1999) Cortical surface-based analysis. I. Segmentation and surface reconstruction. *NeuroImage* 9: 179–194. PMID: [9931268](#)
29. Miller KJ, Hebb AO, Hermes D, Nijs MD, Ojemann JG, et al. Brain surface electrode co-registration using MRI and x-ray; 2010. IEEE. pp. 6015–6018.
30. Schalk G, McFarland DJ, Hinterberger T, Birbaumer N, Wolpaw JR (2004) BCI2000: a general-purpose brain-computer interface (BCI) system. *IEEE Trans Biomed Eng* 51: 1034–1043. PMID: [15188875](#)
31. Porat B (1997) A course in digital signal processing: Wiley.
32. Miller KJ, Hermes D, Honey CJ, Hebb AO, Ramsey NF, et al. (2012) Human motor cortical activity is selectively phase-entrained on underlying rhythms. *PLoS computational biology* 8: e1002655. doi: [10.1371/journal.pcbi.1002655](https://doi.org/10.1371/journal.pcbi.1002655) PMID: [22969416](#)
33. Miller KJ, Hermes D, Honey CJ, Sharma M, Rao RP, et al. (2010) Dynamic modulation of local population activity by rhythm phase in human occipital cortex during a visual search task. *Frontiers in human neuroscience* 4: 197. doi: [10.3389/fnhum.2010.00197](https://doi.org/10.3389/fnhum.2010.00197) PMID: [21119778](#)
34. Hermes D, Miller KJ, Wandell BA, Winawer J (2014) Stimulus Dependence of Gamma Oscillations in Human Visual Cortex. *Cereb Cortex*.
35. Guyon I, Elisseeff A (2003) An Introduction to Variable and Feature Selection. *Journal of Machine Learning Research* 3: 1157–1182.
36. Bishop CM (1995) Neural networks for pattern recognition: Oxford university press.
37. Keysers C, Xiao DK, Foldiak P, Perrett DI (2001) The speed of sight. *J Cogn Neurosci* 13: 90–101. PMID: [11224911](#)
38. Burr DC, Santoro L (2001) Temporal integration of optic flow, measured by contrast and coherence thresholds. *Vision research* 41: 1891–1899. PMID: [11412882](#)
39. Holcombe AO (2009) Seeing slow and seeing fast: two limits on perception. *Trends in cognitive sciences* 13: 216–221. doi: [10.1016/j.tics.2009.02.005](https://doi.org/10.1016/j.tics.2009.02.005) PMID: [19386535](#)
40. McKeeff TJ, Remus DA, Tong F (2007) Temporal limitations in object processing across the human ventral visual pathway. *J Neurophysiol* 98: 382–393. PMID: [17493920](#)
41. Rolls ET, Tovee MJ (1994) Processing speed in the cerebral cortex and the neurophysiology of visual masking. *Proc Biol Sci* 257: 9–15. PMID: [8090795](#)
42. Geman S, Bienenstock E, Doursat R (1992) Neural networks and the bias/variance dilemma. *Neural computation* 4: 1–58.
43. Geurts P (2010) Bias vs Variance Decomposition for Regression and Classification. *Data Mining and Knowledge Discovery Handbook*: Springer. pp. 733–746.
44. Apple (2011) Dictionary.

45. Hung CP, Kreiman G, Poggio T, DiCarlo JJ (2005) Fast readout of object identity from macaque inferior temporal cortex. *Science* 310: 863–866. PMID: [16272124](#)
46. Liu H, Agam Y, Madsen JR, Kreiman G (2009) Timing, timing, timing: fast decoding of object information from intracranial field potentials in human visual cortex. *Neuron* 62: 281–290. doi: [10.1016/j.neuron.2009.02.025](#) PMID: [19409272](#)
47. Thor DH (1967) Dichoptic viewing and temporal discrimination: an attempted replication. *Science* 158: 1704–1705. PMID: [6059654](#)
48. Honey C, Kirchner H, VanRullen R (2008) Faces in the cloud: Fourier power spectrum biases ultrarapid face detection. *Journal of vision* 8: 9 1–13.
49. Kirchner H, Thorpe SJ (2006) Ultra-rapid object detection with saccadic eye movements: visual processing speed revisited. *Vision research* 46: 1762–1776. PMID: [16289663](#)
50. Crouzet SM, Kirchner H, Thorpe SJ (2010) Fast saccades toward faces: face detection in just 100 ms. *Journal of vision* 10: 16 11–17.
51. Smallwood J, Davies JB, Heim D, Finnigan F, Sudberry M, et al. (2004) Subjective experience and the attentional lapse: task engagement and disengagement during sustained attention. *Conscious Cogn* 13: 657–690. PMID: [15522626](#)
52. Honey CJ, Thesen T, Donner TH, Silbert LJ, Carlson CE, et al. (2012) Slow cortical dynamics and the accumulation of information over long timescales. *Neuron* 76: 423–434. doi: [10.1016/j.neuron.2012.08.011](#) PMID: [23083743](#)
53. Mesgarani N, Cheung C, Johnson K, Chang EF (2014) Phonetic feature encoding in human superior temporal gyrus. *Science* 343: 1006–1010. doi: [10.1126/science.1245994](#) PMID: [24482117](#)
54. Abel TJ, Rhone AE, Nourski KV, Kawasaki H, Oya H, et al. (2015) Direct physiologic evidence of a heteromodal convergence region for proper naming in human left anterior temporal lobe. *J Neurosci* 35: 1513–1520. doi: [10.1523/JNEUROSCI.3387-14.2015](#) PMID: [25632128](#)
55. Sun H, Blakely TM, Darvas F, Wander JD, Johnson LA, et al. (2015) Sequential activation of premotor, primary somatosensory and primary motor areas in humans during cued finger movements. *Clin Neurophysiol*.
56. Miller KJ, Hermes D, Pestilli F, Wig GS, Rao RPN, et al. (2015) Face percept formation in human ventral temporal cortex. In submission.
57. Mitzdorf U (1985) Current Source-Density Method and Application in Cat Cerebral-Cortex—Investigation of Evoked-Potentials and Eeg Phenomena. *Physiological Reviews* 65: 37–100. PMID: [3880898](#)
58. VanRullen R, Thorpe SJ (2002) Surfing a spike wave down the ventral stream. *Vision Res* 42: 2593–2615. PMID: [12446033](#)

**Spontaneous Decoding of the Timing and Content of Human Object Perception from Cortical Surface Recordings Reveals Complementary Information in the Event-Related Potential and Broadband Spectral Change**

KJ Miller, G Schalk, D Hermes, JG Ojemann, RPN Rao

---

**Content:**

- **Supporting Information Table S1:** Participant characteristics, and number of selected electrodes by  $r^2 < 0.05$  criteria (from first fold only)
  - **Supporting Information Text S1 -** Power spectral analysis:
  - **Supporting Information Text S2 -** Decoupling the cortical spectrum:
  - **Supporting Information Table S2:** Correct classifications, when the timing of events is pre-designated.
  - **Supporting Information Table S3:** Errors for Spontaneous Predictions
  - **Supporting Information Figure S1:** Choice of collision time does not inform classifier about timing of events.
- 

subject	age	sex	Total	Rejected	Remaining	ERP-responsive			ERBB-responsive		
						joint	face	house	joint	face	house
1	37	M	63	3	60	29	5	3	2	2	1
2	31	M	50	0	50	5	3	0	5	2	0
3	45	F	64	6	58	10	2	2	2	2	0
4	32	M	64	6	58	6	11	0	3	4	1
5		F	44	5	39	18	2	5	7	2	0
6	27	F	36	5	31	21	3	0	12	2	1
7	23	M	64	12	52	12	15	4	1	7	1

**Supporting Information Table S1:** Participant characteristics, and number of selected electrodes by  $r^2 < 0.05$  criteria (from first fold only)

## Supporting Information Text S1 - Power spectral analysis:

Power spectral analysis (for both power spectral snapshots and wavelet decomposition) was performed for frequencies between 1 and 200 Hz, in 1Hz bins, excepting line noise at 60Hz harmonics (57-63Hz, 117-123Hz, 177-183Hz).

**Power spectral snapshots:** A set of epochs surrounding the middle of each face or house visual stimulus and each inter-stimulus-interval (ISI) period,  $\tau_q$ , were extracted from  $V(t)$ ; each epoch was of duration  $T = 1\text{s}$ ,  $\left(\tau_q - \frac{1}{2}T\right) < t < \left(\tau_q + \frac{1}{2}T\right)$ . The power spectral density (PSD) of the epoch flanking time  $\tau_q$  was calculated as

$$P(f, q) = \left| \frac{1}{\sqrt{T}} \sum_{t=-T/2}^{+T/2} V(\tau_q + t) H(t) e^{i2\pi ft} \right|^2$$

with Hann window (42)

$$H(t) = \frac{1}{2} \left( 1 + \cos\left(\frac{2\pi t}{T}\right) \right).$$

**Wavelet approach:** A Morlet wavelet (43) of the form:  $\psi(\tau, t) = \exp\frac{i2\pi t}{\tau} \exp\frac{-t^2}{2\tau^2}$  was convolved with the timeseries to get a time-frequency estimate for every  $f = 1/\tau$ :

$$\tilde{V}(1/\tau, t) = \sum_{t'=-5\tau/2}^{5\tau/2} V(t+t') \psi(t', \tau)$$

A total of 5 cycles ( $5\tau$ ) were used to estimate the amplitude and phase of the signal at each frequency for every point in time. In this way, a time-varying Fourier component  $\tilde{V}(f, t) = r(f, t) e^{iq(f, t)}$ , with fixed uncertainty between the confidence in the estimate of the instantaneous amplitude and phase versus the confidence in temporal resolution is obtained at each frequency.

## **Supporting Information Text S2 - Decoupling the cortical spectrum:**

The decoupling process to separate rhythmic activity from broadband change is described and illustrated in detail in (25), and illustrated specifically for this face-house context in (12). It was applied here as follows:

**Principal component decomposition of spectral change:** The samples of the PSD,  $P(f,q)$ , (total  $N_q$ ), were normalized prior to decomposition:

$\hat{P}(f,q) = \ln(P(f,q)) - \ln\left(\frac{1}{N_q} \sum_q P(f,q)\right)$ . A PCA method was used to determine the eigenvalues  $\lambda_j$  and eigenvectors  $\vec{e}_j$  of the correlation matrix:  $C(f,f') = \sum_q \hat{P}(f,q) \hat{P}(f',q)$ .

These eigenvectors,  $\hat{C} \vec{e}_j = \lambda_j \vec{e}_j$ , the "Principal Spectral Components" (PSCs), reveal which frequencies vary together, and are ordered by magnitude of corresponding eigenvalue:  $\lambda_1 > \lambda_2 > \dots > \lambda_{N_f}$  ( $N_f \equiv$  number of frequencies). If we define the rotation matrix  $A(f,j) = (\vec{e}_1, \vec{e}_2, \dots, \vec{e}_{N_f})$ , then the projection,  $W(j,q)$ , of each individual original spectrum in the ensemble onto the new basis is  $W(j,q) = \sum_f A(j,f) \hat{P}(f,q)$ .

**The timecourse of broadband spectral change:** The time-dependent, normalized, dynamic spectrum,  $\hat{P}(f,t)$ , can be obtained in parallel fashion to the spectral snapshots.

$P(f,t) = \frac{|\tilde{V}(f,t)|^2}{\frac{1}{N_t} \sum_t |\tilde{V}(f,t)|^2}$ , and  $\hat{P}(f,t) = \ln(P(f,t)) - \ln\left(\frac{1}{N_t} \sum_t P(f,t)\right)$ . The reflection of

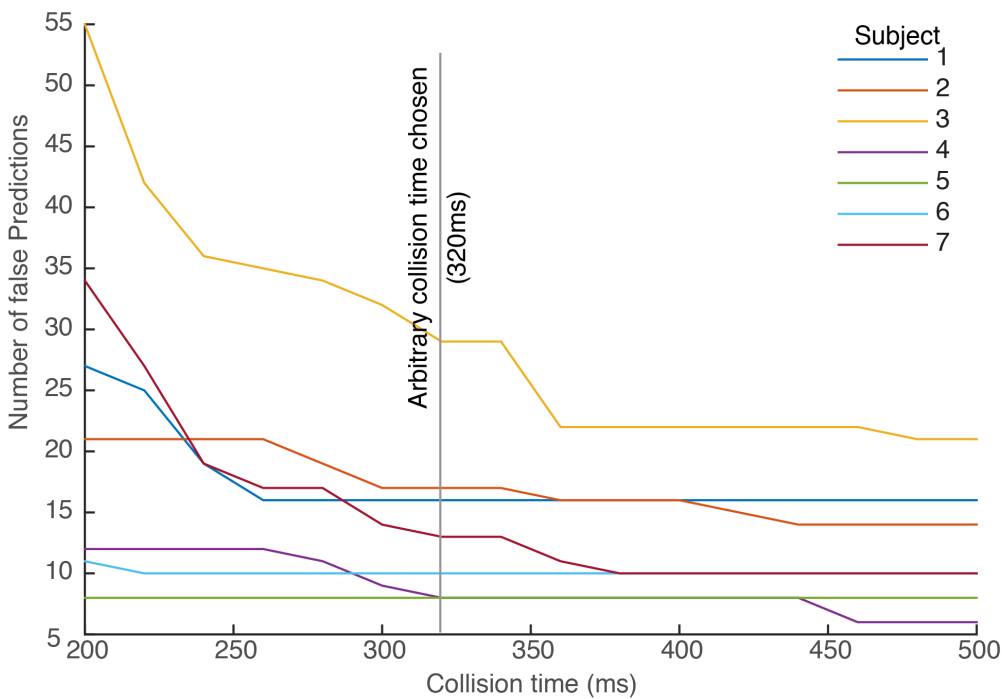
the 1<sup>st</sup> PSC ( $\vec{e}_1$ ) in the dynamic spectrum can be estimated by projecting the dynamic spectrum onto it:  $\ln A(t) = \sum_f e_1(f) \hat{P}(f,t)$ . We call it  $\ln A(t)$  here, because it approximates the logarithm of the time course of the coefficient of a power law in the cortical spectrum of the form  $P(f,t) = A(t) f^{-\gamma}$  (25). The "broadband timecourse" for electrode  $n$  is obtained by smoothing  $\ln A(t)$  with a Gaussian filter of standard deviation 80ms and then z-scoring (to put in intuitive units, because this measure is approximately normally distributed (44)), exponentiating, and subtracting 1 (so that it takes on a baseline value of 0):  $B_n(t) = \exp(\ln A_n^Z(t)) - 1$ . The broadband power time course is meant to function as a time-varying estimate of changes in a multiplicative factor in the population firing rate (11, 25).

	Subject 1		Subject 2		Subject 3		Subject 4		Subject 5		Subject 6		Subject 7	
	Faces	Houses												
ERP	127	144	128	145	85	145	137	149	145	142	145	144	107	146
ERBB	141	150	149	147	143	150	150	150	140	147	141	140	137	150
Both	139	147	150	150	124	149	150	150	145	148	147	144	137	150

**Supporting Information Table S2:** Correct classifications, when the timing of events is pre-designated, sorted by stimulus type (note that each number is out of a possible 150 correct).

		Number of captured stimuli (by time or class)						Average absolute value of temporal error (for correct captures)					
		All	Face	House	All	Time	Class	House	All	Face	House	Face	House
Subject 1	ERP	268 / 300	141 / 150	127 / 150	33	4/23	23/23	1/10	9/10	19ms +/-14, (offset -2)	17ms +/-12, (offset 3)	22ms +/-16, (offset -7)	
	ERBB	266 / 300	130 / 150	136 / 150	55	3/3	0/3	37/52	21/52	32ms +/-33, (offset 10)	27ms +/-25, (offset 9)	37ms +/-38, (offset 11)	
	Both	281 / 300	144 / 150	137 / 150	16	0/10	10/10	0/6	6/6	18ms +/-13, (offset -1)	17ms +/-12, (offset 4)	19ms +/-13, (offset -6)	
Subject 2	ERP	278 / 300	135 / 150	143 / 150	35	6/8	6/8	12/27	18/27	25ms +/-26, (offset 10)	20ms +/-15, (offset 12)	29ms +/-32, (offset 7)	
	ERBB	291 / 300	144 / 150	147 / 150	8	2/2	1/2	3/6	3/6	35ms +/-30, (offset 18)	26ms +/-21, (offset 5)	44ms +/-35, (offset 31)	
	Both	290 / 300	145 / 150	145 / 150	12	4/4	4/4	6/8	2/8	19ms +/-18, (offset 9)	17ms +/-13, (offset 8)	22ms +/-21, (offset 11)	
Subject 3	ERP	241 / 300	143 / 150	98 / 150	74	15/60	56/60	11/14	5/14	20ms +/-16, (offset -2)	17ms +/-11, (offset -4)	24ms +/-20, (offset 2)	
	ERBB	275 / 300	142 / 150	133 / 150	34	3/3	0/3	31/31	4/31	30ms +/-26, (offset 4)	20ms +/-14, (offset 4)	39ms +/-32, (offset 3)	
	Both	285 / 300	144 / 150	141 / 150	23	7/15	12/15	5/8	5/8	19ms +/-15, (offset 1)	17ms +/-11, (offset -3)	22ms +/-17, (offset 5)	
Subject 4	ERP	290 / 300	150 / 150	140 / 150	18	1/10	10/10	8/8	1/8	18ms +/-15, (offset -2)	17ms +/-11, (offset -2)	20ms +/-19, (offset -2)	
	ERBB	276 / 300	143 / 150	133 / 150	35	4/9	9/9	21/26	7/26	38ms +/-35, (offset 1)	24ms +/-20, (offset 2)	53ms +/-41, (offset 1)	
	Both	295 / 300	150 / 150	145 / 150	8	1/2	2/2	6/6	0/6	19ms +/-17, (offset -4)	17ms +/-11, (offset -4)	21ms +/-21, (offset -4)	
Subject 5	ERP	293 / 300	148 / 150	145 / 150	7	0/5	5/5	0/2	2/2	18ms +/-12, (offset -7)	18ms +/-13, (offset -10)	18ms +/-11, (offset -5)	
	ERBB	283 / 300	139 / 150	144 / 150	17	0/6	6/6	0/11	11/11	25ms +/-19, (offset -2)	23ms +/-16, (offset 14)	27ms +/-21, (offset -18)	
	Both	291 / 300	150 / 150	141 / 150	8	0/8	8/8	0/0	0/0	18ms +/-12, (offset -7)	18ms +/-12, (offset -8)	18ms +/-12, (offset -7)	
Subject 6	ERP	286 / 300	142 / 150	144 / 150	18	4/10	7/10	3/8	5/8	20ms +/-15, (offset -7)	19ms +/-15, (offset -5)	20ms +/-15, (offset -9)	
	ERBB	266 / 300	139 / 150	127 / 150	35	0/21	21/21	3/14	11/14	27ms +/-20, (offset -5)	21ms +/-15, (offset 9)	34ms +/-22, (offset -21)	
	Both	290 / 300	147 / 150	143 / 150	10	0/7	7/7	0/3	3/3	21ms +/-17, (offset -5)	20ms +/-18, (offset 3)	22ms +/-16, (offset -14)	
Subject 7	ERP	266 / 300	143 / 150	123 / 150	52	11/30	28/30	17/22	10/22	22ms +/-22, (offset 1)	19ms +/-19, (offset 1)	26ms +/-25, (offset 2)	
	ERBB	281 / 300	135 / 150	146 / 150	17	4/4	1/4	3/13	11/13	34ms +/-34, (offset 21)	20ms +/-18, (offset 7)	48ms +/-39, (offset 34)	
	Both	291 / 300	142 / 150	149 / 150	10	1/1	0/1	2/9	7/9	21ms +/-19, (offset 4)	18ms +/-16, (offset 4)	24ms +/-22, (offset 5)	

**Supporting Information Table S3:** Errors for Spontaneous Predictions



**Supporting Information Figure S1:** Number of false predictions as a function of the choice of maximum distance between predicted event times (Collision time), for classification using both ERP and ERBB. The monotonic decay form and lack of “dips” or “peaks” shows that the collision time chosen did not inform the classifier about timing of stimuli. Of note, subject 5, who had the most early visual electrodes, was unaffected by even very low collision times. The number of events correctly predicted was the same for every choice of collision time, so those data are not shown.